Journal of Materials Chemistry A

Accepted Manuscript

ROYAL SOCIETY OF CHEMISTRY

www.rsc.org/materialsA

Recent progress on electrocatalysts with mesoporous structure for application in polymer electrolyte membrane fuel cells

Wei Xu [a,b], Zucheng Wu [b] and Shanwen Tao [a,c*]

[a] School of Engineering, University of Warwick, Coventry CV4 7AL, UK

[b] Department of Environmental Engineering, State Key Laboratory of Clean Energy Utilization, Zhejiang University, Hangzhou 310058, Zhejiang, China

[c] Department of Chemical Engineering, Monash University, Clayton, Victoria 3800, Australia

---

Abstract: Recently mesoporous materials have drawn great attention in fuel cell related applications, such as preparation of polymer electrolyte membranes and catalysts, hydrogen storage and purification. In this mini-review, we focus on recent development in mesoporous electrocatalysts for polymer electrolyte membrane fuel cells, including metallic and metal-free catalysts for use as either anode or cathode catalysts. Mesoporous Pt-based metals have been synthesized as anode catalyst with improved activity and durability. Mesoporous carbons together with other inorganic materials are better supporting materials than conventional carbon black, which have large surface area, high porosity and synergistic effect with metal particles. Pt supported on these materials possesses small particle size, uniform distribution and good access to fuels, which performs better as fuel cell catalysts than commercial Pt/C. Some efforts such as further improvement in the conductivity and chemical stability of mesoporous carbon by chemical doping are stated. Moreover, metal free cathode catalysts based on heteroatoms modified mesoporous carbon are also summarized.

Keywords: review, mesoporous, catalyst, fuel cell

---

* Corresponding author:
School of Engineering, University of Warwick, Coventry CV4 7AL, UK
E-mail: S.Tao.1@warwick.ac.uk
Tel: +44 (0)24 761 51680
Fax: +44 (0)24 764 18922
E-mail: S.Tao.1@warwick.ac.uk

1. Introduction

Polymer electrolyte membrane fuel cells (PEMFCs) based on either proton exchange membrane (acidic condition) or anion exchange membrane (alkaline condition) can use a wide range of renewable resources such as hydrogen gas, methanol, ethanol, formic acid, ammonia, hydrazine, urea etc. as fuels[1-6]. They demonstrate outstanding energy density among the electrochemical energy conversion and storage systems, which is about 5 times larger than that for current Li-ion batteries[7]. Due to the diversity of energy resources and high energy density, PEMFCs are promising for applications in vehicles, portable electronic devices and environmental technology to produce clean energy[1, 8-10]. The main barriers of scaling-up PEMFCs are cost (e.g. hydrogen storage, ion exchange membrane, catalysts) and durability of ion exchange membrane, catalysts, flow conditions[11]. According to the U.S. Department of Energy (DOE), targets of hydrogen storage capacity and fuel cell system cost are 40 kg m^{-3} and \$40 kW^{-1} respectively by 2020[12, 13]. The core components of fuel cell system are polymer electrolyte membrane, catalysts layer and gas diffusion layer constituting the membrane electrolyte assembly (MEA). The MEA is reported to be accounting for about 35~50% of the cost of fuel cell system[13]. As a consequence, the MEA cost needs to be reduced by 27% to achieve the target in 2020. Another problem is fuel cell durability, which mainly comes from membrane dehydration and catalysts degradation because of poisoning, corrosion and fuels crossover. Developing new materials for MEA is a hot topic in fuel cell research to reduce cost and improve durability.

Since the ExxonMobil's M41S series of mesoporous molecular sieves[14] were first reported, researches on mesoporous materials have been growing for decades. Mesoporous materials are fascinating in many research areas due to the wonderful porosity structures such as tunable pore diameters, high surface areas, alternative pore shape, and abundant compositions[15]. Different mesoporous composites like silica-based (SiO_2, MCM-41 and SBA-15 series), inorganic (metal oxides, carbon) and organic-inorganic (organometallics, colloids and nano-objects, coordination polymers) are developed with specific functions to meet the needs in different applications[15, 16]. Recently, mesoporous materials have shown excellent performance on the applications in PEMFCs. For instance, *Meso*-silica has been used for synthesis of ion exchange membrane by incorporating acidic functional group such as phosphotungstic acid, phosphoric acid, sulfonated benzene, etc[17-20]. The tested membrane conductivity is comparable to Nafion® membrane and increases with temperature up to 200 ºC. Moreover, the mesoporous membrane can obviously prevent the crossover of liquid fuel (e.g. methanol, ethanol). Mesoporous materials have been intensively studied in energy conversion technologies[16]. The mesopores (2-50 nm in pore size) network can enhance the intracrystalline

diffusion over orders of magnitude to improve mass transport, compared to diffusivity in the continuous micropore (< 2 nm in pore size) space[21]. The molecular exchange rate of materials traversed by mesopores network is accelerated by using pulsed field gradient (PFG) technique of nuclear magnetic resonance (NMR) for quantitative intracrystalline diffusion measurement. The details on mass transport of mesoporous materials have been covered in excellent reviews[21, 22]. In fuel cells field, the conductive mesoporous materials, especially the mesoporous carbon, have been intensively investigated to prepare electrocatalysts for electrodes, in order to overcome the challenge of cost and durability of the commercial Pt/C catalyst. Mesoporous structures have advantages of large specific surface area, appropriate pore sizes (2 to 50 nm) and large pore volumes for fuels transfer and particles deposition. Thus it is a promising method to obtain highly stable and active catalysts for fuel cells. In the aspect of anode catalysts, strategies include direct synthesis of mesoporous Pt and Pt alloys without supports, or formation of metallic nanoparticles on mesoporous supports (e.g. carbon, metal oxide, and metal nitride). As for cathode, metal based catalysts with mesoporous supports, as well as heteroatoms doped mesoporous carbons as metal-free catalysts are both widely reported. Although there are a few excellent reviews about applications of mesoporous materials in wide topics of energy conversion and storage such as solar cells, fuel production, rechargeable batteries, supercapacitors and fuel cells[16, 23-28], this review focuses on recent development of mesoporous materials for fuel cells catalysts, including mesoporous Pt (and Pt alloys), metals with mesoporous supports, and metal-free mesoporous carbon catalysts.

2. Use of mesoporous materials as anode catalysts

Platinum–group metals are tested to be the most active catalysts toward both anode oxidation reaction and cathode reduction reaction. The challenges of Pt catalysts are high cost and poisoning by the oxidation intermediates like CO_{ads} and N_{ads}[29, 30]. Numerous works have been done to improve the activity and durability of noble Pt-based catalysts by doping non-noble elements (e.g. transition metals, phosphorus) and forming hollow, core-shell or mesoporous nanostructures[31-33]. Efforts on mesoporous electrocatalysts are basically in two approaches: directly prepare unsupported metal electrocatalysts with mesoporous structure to obtain large surface area; enhance the dispersion of metal particles by depositing metals on mesoporous supporting materials.

2.1 Metallic mesoporous electrocatalysts

Metallic mesoporous electrocatalysts (MMECs) have a much larger electrochemically active surface area (ECSA) than conventional solid catalysts[5]. In addition, the porous structure with optimal pore size can improve the mass transport of fuels[34]. Consequently, related results presented by Yusuke

Yamuchi show much better performances of mesoporous Pt than Pt black in methanol electrooxidation reaction under acidic condition[35, 36]. The MMECs are usually synthesized via liquid crystalline templating methods. A facile way of preparing metallic MMECs has received more and more attention by using surfactant as soft-template[16]. Low molecular weight surfactants can result in large surface area due to small pore size, but on the other hand mass transfer of fuels to catalysts active sites will be inadequate. Large molecular weight surfactant such as triblock copolymers can lead to a large pore size by forming ‘‘cavity-crystals’’. Metal ions are mixed with soft-template via surfactant self-assembly, and then reduced to nanocomposites by chemical or electrochemical reduction. Finally the nanocomposites are washed to remove the surfactant and remain MMECs.

Bimetallic Pt alloys are common strategies to achieve better activity and resistance to adsorbed intermediates poisoning[4, 37]. Due to the mesoporous structure, the performance of Pt alloys has been further improved. For methanol electrooxidation, mesoporous Pt (16 m^2 g^{-1}) and PtRu (20 m^2 g^{-1}) with a pore diameter of ~10 nm are prepared by electrodeposition with Pluronic F127® as surfactant. The long limit mass activities reach 2.42 and 7.52 A g^{-1} for Pt and PtRu, which are higher than the commercial Pt/C catalyst (2.29 A g^{-1})[34]. Mesoporous PtCo nanorods with a pore diameter of 10~14 nm, are electrodeposited in the interior channels of porous membrane with metal precursors dissolved in water-ionic liquid microemulsion[38, 39]. The porosity of PtCo is dependent on the ratio of water to ionic liquid, and the diameters of nanorods are in accordance with the pore size of membrane. It is claimed that the PtCo nanorods have ECSA of about 40~200 m^2 g^{-1}, and 3 times higher mass-normalized current density than commercial Pt/C with improved poisoning tolerance. For ethanol electrooxidation, mesoporous PtRuSn prepared by the reduction of metal precursors with non-ionic surfactant achieves active surface area of 54 m^2 g^{-1}, and lowers onset potential by about 0.1 V [40]. Current density of PtRuSn in 0.5 M H_2SO_4/1 M C_2H_5OH reaches about 20 A g^{-1} at 0.6 V vs. RHE. In practice, metal particles formed with small size (usually around several nm) are beneficial for larger active surface areas and better activity[41]. However the pore size of MMECs does not have a similar effect as particle size. Mesoporous PtRu with pore size of 10 nm is observed to be better than that with pore size of 3 nm in methanol oxidation[42]. The possible reason is that methanol residence time is not enough owing to the poor mass transfer if pore size is less than 3 nm [43]. On the contrary, catalysts with 10 nm pore size have greater accessibility of methanol, thus methanol can be adequately oxidized in larger pores. It indicates that the pore size of MMECs is an important factor.

2.2 Metals supported on mesoporous materials (MSMMs)

Another strategy of preparing mesoporous electrocatalyst for fuel cell anode is to deposit metals on mesoporous materials. In comparison with MMECs, mesoporous catalysts for fuel cells are mainly focused on MSMMs according to published works. In particular, supporting materials such as carbon black for metal catalysts have been commonly used to prepare electrodes in fuel cells fabrication.

Carbon supporting materials have large surface area, high electrical conductivity, so they can greatly improve the performance of catalysts[43]. With development of carbon supported catalysts, the loading of noble metals in fuel cells have been largely reduced. However, traditional carbon supporting materials still face some disadvantages. First, carbon black is susceptible to corrosion caused by electrochemical oxidation[44, 45]. Second, the size of micropores (less than 1 nm) in carbon is too small to obtain enough mass transfer of fuel to the catalysts surface, thus limiting the activity of the catalyst[46, 47]. In the same way, these micropores will result in low accessible surface area to support the metal deposition, so metal particles primarily reside on the outer carbon black surface. Third, carbon black is poor to gases and liquids diffusion and does not conduct protons, leading to low catalyst utilization. Accordingly, ionomers like expensive Nafion® inks are always used to increase the three-phase boundary and facilitate transport of protons[48].

In order to solve above problems, novel supporting materials are applied with the development of advanced nanomaterials. For example, graphene, carbon nanotubes and mesoporous carbon have been used to prepare metal based catalysts for fuel cells and exhibit improved electrochemical properties due to large surface area, high chemical stability and excellent electrical conductivity[49-52]. The pore size of mesoporous materials (2 to 50 nm) matches with most metal particles, leading to high accessible surface area to support metals deposition. Besides, the relative large pores (>3 nm) are able to allow fuels to contact metals surface with long residence time, resulting in a high utilization of metals and high oxidation efficiency. Although the commercial ordered mesoporous silica (OMS) is proved to be an ideal supporting material in environment- and energy-related catalysis, the poor electrical conductivity limits its direct application in fuel cells[53, 54]. Based on silica template, mesoporous carbon materials were first prepared in 1999, which had great scientific and technological importance as new electrode materials to be applied in fuel cells[55]. Present researches are mostly concentrated on ordered mesoporous carbons (OMCs).

The hard-template (e.g. SBA-15, MCM-41 and silica colloid) and soft-template (e.g. amphiphilic surfactants and triblock co-polymers) are two widely used synthesis methods of OMCs. In hard-template method, pores in OMS are mixed with carbon source (e.g. sucrose, resorcinol and formaldehyde). Then the carbonization is completed by pyrolysis at high temperature, followed by removing silica template to get OMCs. In soft-template method, carbon precursor (organic monomers) is polymerized with the self-assembly of surfactant in liquid to form carbon-surfactant composite. After removing surfactant, carbonization will be carried out by pyrolysis at high temperature. Schematic diagrams of the two synthesis methods are shown in Fig. 1[56]. Both methods to make carbon based mesoporous supporting materials require a pyrolysis process (normally at 900~1000 ºC under N_2 atmosphere) to graphitize carbon precursor. Mesoporous carbon nanoparticles also can be prepared with glucose as carbon precursor partially carbonized at 180 ºC for 4 h, followed by functionalization

with amine-terminated ionic liquid[57]. Finally, metal ions are reduced and deposited on OMCs to get MSMMs.

Until now, different kinds of MSMMs have been successfully synthesized. In Ahn *et al.*'s experiment, colloidal silica was used as template and sucrose was used as carbon source to get 50 wt.% Pt/OMCs[58]. Half of the pores of OMCs (~5 nm diameter) are uniformly occupied by Pt nanoparticles (~2.5 nm particle size) or are lost during Pt/OMC preparation. In addition to the enhanced metals-accommodation ability, mesoporous carbon also leads to better mass transport according to the polarization plots and electrochemical impedance spectroscopy (EIS) results[59]. He *et al.* have investigated the cyclic voltammograms (CVs) of methanol oxidation on commercial Pt/C (E-TEK) and Pt/mesoporous carbon nano particles (Pt/MCNPs)[57]. In the forward scan, the maximum current density of Pt/MCNPs is 2.3 times higher than that of E-TEK Pt/C catalyst. Lee *et al.* use SBA-15 as template to prepare OMCs supported Pt-Ru for methanol oxidation, achieving specific surface area about 900 m^2 g^{-1} and pore size about 4 nm[60]. The specific surface area of OMCs is much larger than that of commercial carbon supports (about 240 m^2 g^{-1}, Vulcan XC-72R)[61]. TEM images show the Pt-Ru nanoparticles are uniformly deposited on OMCs and the particle sizes are limited to 4 nm. They further prepared O-doped OMCs by H_2O_2 treatment to improve the activity. N-doped mesoporous carbons are also developed by using nitrogen-containing carbon precursors such as polyacrylonitrile, polypyrrole and polyaniline[62-65]. Zhang *et al.* developed a honeycomb-like mesoporous N-doped carbon supported Pt catalysts for methanol oxidation[66]. Cyclic voltammogram measurements indicate that peak current density of N-doped carbon catalyst is 1.4 times higher than that of carbon catalyst without N doping. The addition of nitrogen element not only has intense anchoring effect of Pt nanoparticles, but also enhances electric conductivity. The doping of P heteroatom inhibits the aggregation of metal particles and leads to a uniform distribution on mesoporous carbons, clearly presented in TEM pictures in Fig. 2E contrasting with Fig. 2F [67]. The Pt supported on phosphorus doped OMCs (Pt/P_7OMCs) demonstrates much higher current density than Pt/OMCs, Pt/Vulcan XC-72 and PtRu/XC in chronoamperometry (see Fig. 2B). Pt/P_7OMCs has a relatively stable electrochemical activity and better CO-tolerance towards methanol oxidation. One reason may be the increase of oxygen-containing functional groups after P doping, which promote the CO-tolerance and enhance stability. It was found from Fig. 2C that ECSA (90.7 ± 6.1 m^2 g^{-1}) after 10000 s stability test is only a little bit lower than the original value (96.3 ± 7.3 m^2 g^{-1}), and from Fig. 2D that Pt nanoparticles are not obviously aggregated after 10000 s. Moreover, mesoporous carbons incorporated with other compounds, such as ceria, carbon nanotubes, tungsten carbide and tin oxide are also prepared [68-71]. Ceramic materials such as ceria and tungsten carbide were observed to have stabilization effect on Pt during long time test [68, 69]. Stability tests indicate that the electrochemically active surface of Pt/mesoporous carbon-ceria reduces by 45% after accelerated degradation of 2000 min, in comparison to 70% of conventional Pt/C [69]. Tin oxide is also regarded to enhance the ethanol

oxidation on Pt by effectively splitting the C-C bonds in ethanol [71]. Pt on carbon nanotubes doped OMCs (Pt/CNTs-OMC) made by Zhang *et al.* exhibits about twice higher current density in methanol oxidation than Pt/CNTs and Pt/OMC (see Fig.3) [70]. This is because that the doping of CNTs forms unique structure of CNTs–OMC nanocomposites, which are conducive to electron transfer across the OMC particles and result in lowering of the interfacial resistance, illustrated in Fig. 3e. Accordingly, the conductivity of OMC is only 4.3 S m^{-1}, and it rises to 26.4 S m^{-1} after doping CNTs. The ECSAs of Pt/OMCs, Pt/CNTs and Pt /CNTs-OMCs are 57.8, 80.4 and 113.4 m^2 g^{-1}, respectively. In brief, all these doped mesoporous carbons present further improvement of activity and durability of Pt-based catalysts for oxidation reaction in comparison with non-doped mesoporous carbon which are big advantages for fuel cell applications.

Besides carbon-based mesoporous supporting materials, non-carbon mesoporous supporting materials (e.g. CrN, TiN, SnO_2-Sb) have also been developed for Pt. Similarly, these supports have large surface area due to the porous structure. Gurrola *et al.* claim that after 100 cycles of CVs in acid, ECSA of Pt/Sb-SnO_2 decreases less than 10%[72]. In contrast, ECSA of Pt/C decreases significantly attributing to the oxidation of carbon supports. In addition, metal nitride is a better choice for non-carbon supporting materials, as it not only exhibits long-time stability and faster oxidation of CO, but also has high electrical conductivity. Mesoporous TiN is prepared by Yang *et al.* via a solid-solid phase separation method [73]. This material is formed by heating Zn_2TiO_4 under ammonia gas without template. Mesoporous TiN demonstrates high conductivity of 395 S cm^{-1} at 35 bar and good electrochemical stability. Accounting to the CV tests of methanol oxidation, the peak current density of Pt/TiN is 1.5 times higher than that of Pt/C. Yang *et al.* also prepared mesoporous CrN with high conductivity of 54 S cm^{-1} by ammonolysis of $K_2Cr_2O_7$[74]. The pore size ranges from 10 to 20 nm, and some microporosity is observed. CrN is electrochemically stable at acid condition up to 1.2 V, where carbon materials tend to corrode. When used as Pt supporting material (Pt/CrN) for methanol oxidation, the synergistic effect of Pt and CrN allows faster CO oxidation. Peak current density is 195 mA mg_{Pt}^{-1} for Pt/CrN and 145 mA mg_{Pt}^{-1} for Pt/C. Pt/CrN shows higher electrochemical activity and slower deterioration rate than Pt/C. Recently developed mesoporous supports are summarized in Table 1.

Table 1 A summary of properties of various mesoporous supports.

mesoporous supports	specific surface area	pore size	pore volume	conductivity	Ref.
Sb-SnO_2	216.7 m^2 g^{-1}	6.53 nm	0.276 cm^3 g^{-1}	0.202 S cm^{-1}	[72]
CNTs-OMC	1231 m^2 g^{-1}	4.1 nm	1.408 cm^3 g^{-1}	26.4 S m^{-1}	[70]
Ceria-	/	5.1 nm	/	/	[67]

mesocarbon					
N-mesocarbon	639~787 $m^2 g^{-1}$	12.4 nm	/	enhanced by N species	66
P-mesocarbon	1338.8 ± 13 $m^2 g^{-1}$	3.8 ± 0.3 nm	1.36 ± 0.15 $cm^3 g^{-1}$	/	67
SnO_2-mesocarbon	1556 $m^2 g^{-1}$	3.2 nm	/	/	71
CrN	72 $m^2 g^{-1}$	10 to 20 nm	/	54 S cm^{-1} (compressed at 35 bar)	74
TiN	28.1 $m^2 g^{-1}$	25 nm	/	395 S cm^{-1} (at 35 bar)	73
WC/carbon	409 $m^2 g^{-1}$	5.0 nm	0.47 $cm^3 g^{-1}$	/	68

Recently reported MMECs and MSMMs for fuel cell anode, both achieved enhanced specific mass activity and durability which are superior to commercial Pt/C catalysts. MMECs can be prepared in a facile way at room temperature, avoiding the origin of high cost of high-temperature pyrolysis during the MSMMs synthesis. In addition, MMECs also can be directly grown on electrode surface with good contact conditions by electrodeposition method[34, 38, 42], without the use of costly ionomer to immobilize catalysts onto electrode surface. The nanostructure, particle size, pore size and element composition of MMECs and MSMMs can be designed by choosing templates and reaction conditions during synthesis, in order to obtain optimal performance. This provides a promising method for the generation of high-performance and cost-effective metal catalysts for fuel cells with stable performance.

3. Use of mesoporous materials in cathode catalysts

The cathode reaction of oxygen reduction reaction (ORR) is the rate-determining process in PEMFCs, thus there are many investigations into ORR catalysts. The ORR has different reaction routines in acidic and alkaline PEMFCs [75]:

Acidic condition: $O_2 + 4H^+ + 4e^- \rightarrow 2H_2O$ ($4e^-$ pathway) (1)

$O_2 + 2H^+ + 2e^- \rightarrow H_2O_2$ ($2e^-$ pathway) (2)

$H_2O_2 + 2H^+ + 2e^- \rightarrow 2H_2O$ (3)

Alkaline condition: $O_2 + 2H_2O + 4e^- \rightarrow 4OH^-$ ($4e^-$ pathway) (4)

$O_2 + H_2O + 2e^- \rightarrow HO_2^- + OH^-$ ($2e^-$ pathway) (5)

$H_2O + HO_2^- + 2e^- \rightarrow 3OH^-$ (6)

Oxygen can be directly reduced to H_2O or OH^- via a $4e^-$ pathway, or incompletely reduced to H_2O_2 or HO_2^- via a $2e^-$ pathway. In proton exchange membrane fuel cells, H^+ is transported from anode to

cathode to further react with O_2, forming H_2O or H_2O_2. The anion exchange membrane based PEMFCs produce OH^- as charge carriers via ORR to provide an alkaline condition. This will allow the use of nonprecious transition metals based mesoporous catalysts for fuel cells.

3.1 Mesoporous cathode electrocatalysts for acidic PEMFCs

Platinum based metals with carbon supports have good catalytic behaviour toward ORR. Nevertheless, the high cost and activity degradation due to agglomeration of platinum nanoparticles, corrosion of the carbon supports and anode fuels crossover still exist as bottleneck for wide commercial application. Accordingly, numerous efforts have been made to improve the catalyst performance. Similar to anode catalysts, mesoporous carbon is used as supports for Pt. Liu *et al.* prepare mesoporous carbon supported Pt, which exhibits higher mass specific kinetics current density than that of XC-72 carbon supported Pt [76]. The durability is also improved, as electrochemical surface area decreases from 24.5 cm^2 mg_{Pt}^{-1} to 20.6 cm^2 $mg_{Pt}^{-1}$of Pt/mesoporous carbon and from 21.8 cm^2 mg_{Pt}^{-1} to 11.1 cm^2 mg_{Pt}^{-1} of Pt/XC-72 under same condition. Besides, mesoporous carbon supported Pt can inhibit the formation of H_2O_2 with yield of 0.25% in ORR, lower than yield of 1.25% from Pt/C[77].

Modified mesoporous carbons and mesoporous metal nitride supported Pt exhibit much more remarkable improvement. You *et al.* synthesized OMC-SiC composites as support for Pt by a controlled carbothermal reduction process to utilize both the ordered mesopores of OMC and the high electrochemical stability of the SiC materials [78]. The ORR current density using Pt/OMC-SiC shows negligible change (0.16%) after 1000 cycles, while ORR current density using commercial Pt/C decreases by 33.4%. The improvement is attributed to a strong interaction of platinum and Si atom on the surface of carbon frameworks, which makes the catalyst more electrochemically stable. In addition, zirconia with treatment of sulfonated ionomer has been used to modify mesoporous carbon support to form zirconia/ionomer/mesoporous carbon[79]. The mass ORR activity increases from 51 mA mg_{Pt}^{-1} to 74 mA mg_{Pt}^{-1} when ionomer is used to improve availability of protons and enhance O_2 solubility. Yang *et al.* tested non-carbon mesoporous CrN supported Pt as catalyst for ORR [80]. The specific surface area of Pt/CrN is 68.5 ± 0.1 m^2 g^{-1}. Kinetic current density obtained from polarization curves at 0.9 V is 9.1 mA mg_{Pt}^{-1} for Pt/CrN and 5 mA mg_{Pt}^{-1} for commercial Pt/C, respectively. Another non-carbon mesoporous support for oxygen reduction reaction is TiNbN with a pore size of 30-50 nm[81]. Its electrical conductivity reaches 3.9 S cm^{-1}, which is about 2.5 times higher than that of Vulcan XC-72 carbon black (1.5 S cm^{-1}) under the same measurement condition. Though its specific surface area is 45 m^2 g^{-1}, which is smaller than mesoporous carbon support, Pt/TiNbN still exhibits larger kinetic current density (256 mA mg_{Pt}^{-1}) than Pt/C (142 mA mg_{Pt}^{-1}) at 0.9 V. The activity loss of Pt/TiNbN and Pt/C after 5000 cycles is 19.2 % and 29.4% respectively, indicating the stability is improved. In addition, TiNbN is stable both in acidic and alkaline solution.

Transition metal catalysts with mesoporous carbon have been proved to be better than those with carbon black attributing to the increased surface area [82-86]. According to Liang's work, a series of mesoporous carbon supported Co (C-N-Co) catalysts are prepared using different template (Silica colloid, ordered mesoporous silica SBA-15, or montmorillonite)[85]. The ORR activity is found to be proportional to specific surface area, as shown in Fig. 4. As a result, mesoporous carbon supported catalysts (VB12/MMT, VB12/SBA-15, VB12/Silica colloid) perform better than carbon black supported catalyst (VB12/C) due to the surface area increase. Liu *et al*. displays stable and methanol-tolerant ORR catalysts, i.e. Fe carbide supported on N-doped carbon, with high specific area (705 m^2 g^{-1}) and kinetic limiting current density (18.35 mA cm^{-2} at 0.7 V) [87].

3.2 Mesoporous electrocatalysts for alkaline membrane fuel cells

In alkaline PEMFCs, transition metals such as Fe and Co based compounds supported on mesoporous carbons are also investigated as ORR catalysts in order to avoid the use of noble metals [88-92]. Cobalt oxide and cobalt sulfide supported on mesoporous carbon or heteroatoms doped carbon possess comparable or even higher catalytic activity than commercial Pt/C toward ORR [93-96]. In addition, Co based catalysts are remarkably methanol-tolerant and more stable than Pt/C. For example, in chronoamperometric test, when the current of Pt/C decreased by 26%, the current of CoS/N,S codoped porous carbon reduced by only 8% under the same condition [95]. Ni-doped Co_3O_4 nanowire array (n_{Ni}/n_{Co}=1:9) with mesoporous structure was used for ORR by Tong *et al.* recently [97]. This mesoporous Ni-Co_3O_4 has a large pore volume of 0.23 cm^3 g^{-1} with pore size ranging from 4 to 15 nm, leading to a large surface area of 70.3 m^2 g^{-1}. It exhibits more positive half-wave potential ($E_{1/2}$=0.86 V) and higher diffusion-limiting current density (J_L=about 5.76 mA cm^{-2}) than Co_3O_4 ($E_{1/2}$=0.6 V, J_L=1.32 mA cm^{-2}) and Pt/C ($E_{1/2}$=0.85 V, J_L=5.42 mA cm^{-2}) catalysts. It is almost insensitive to methanol and CO, and much more stable than Pt/C in accelerated ORR measurement. Some studies reported Fe based mesoporous catalysts possess high catalytic activity comparable with commercial Pt/C, long-time stability and methanol tolerance [98, 99]. The addition of Fe has been observed to greatly improve the ORR activity of mesoporous carbon with N doping due to high density of surface active sites [98, 99]. When a trace amount of Fe (0.2 at.%) is added, the calculated kinetic current density of Fe-N-C catalyst increases from about 6 mA cm^{-2} (N-C catalyst) to 32.26 mA cm^{-2}, which is higher than Pt/C (30.56 mA cm^{-2})[100]. It was also noticed that the number of ORR electron-transfer changes from 2.61 to 4.04. However, Yang *et al.* found that the role of Fe was to produce more active N sites during the catalysts preparation, and the physical presence of Fe in N-doped carbon was not necessary to enhance the ORR activity [101]. The activity sites of Fe-N-C need to be further investigated. Until now, great improvement of nonprecious metals based ORR catalysts using have been made for both acidic and alkaline PEMFCs, as listed in Table 1, in order to reduce cost and enhance performance.

Table 2 Selected ORR catalysts composed by nonprecious transition metal with mesoporous carbon as a supporting material.

Catalyst	Centred pore diameter (nm)	Specific surface area (m^2 g^{-1})	ORR onset potential	Performance	Ref.
Fe-N/OMC (hollow-core)	3.5	1,187	0.89 V vs. RHE	ORR current densities at 0.8 V vs. RHE are -0.04 mA cm^{-2} for Fe-N/commercial carbon (Ketjen Black CJ600), and -1.0 mA cm^{-2} for Fe-N/OMC	82
Fe-N/OMC	~22	1,138 to 1,338	~0.8 V vs. RHE	ORR current densities at 0.55 V vs. RHE are -1.1 mA cm^{-2} for Fe-N/commercial carbon (Black Pearl 2000), and -1.5 to -3.0 mA cm^{-2} for Fe-N/OMC (depending on pore diameter)	83, 84
Co-N-carbon	12	572	~0.87 vs RHE	4.5 mA cm^{-2} at 0.3 V, better than carbon black supported Co-N	85
CoFe-N-OMC (Co:Fe=1:3)	2.4	670	~0.7 V vs. RHE	When used as cathode catalysts in fuel cell tests, at a cell voltage of 0.3 V, current density of PAIN/CoFe/OMC and commercial Pt/C is 0.89 and 1.07 A cm^{-2}, respectively.	86
Co_3O_4/N-mesoporous graphene	20 to 40	1,599	0.93 V vs RHE	Compared to commercial Pt/C, it has more positive onset potential, higher current density and improved stability from prevention of nanoparticles agglomeration	93
CoO/N-carbon	3.3	1390	-0.06 V vs Ag/AgCl	Kinetic-limited current density reaches 22.29 mA cm^{-2} at -0.4 V, higher than that of commercial Pt/C (21.32 mA cm^{-2}); largely improved methanol tolerant	94
CoS/N,S-carbon	N/A	248	0.92 V vs RHE	ORR current density reaches -4.50 mA cm^{-2} at 0.45 V vs. RHE, largely improved methanol tolerant	95
CoS_2/graphene oxide	2.5 to 3.5	10 to 19	0.97 V vs RHE	ORR potential at -3 mA cm^{-2} is 0.76 V for CoS_2/graphene oxide and 0.86 V for Pt/C	96
Fe_3C@N-carbon	2	705	~0.92 vs RHE	Kinetic limiting current density (18.35 mA cm^{-2}, at 0.7 V) was close to that of commercial Pt/C catalyst (19.25 mA cm^{-2}, at 0.7 V)	87
Fe-N/carbon	6.6	56	0.92 vs RHE	ORR activity is comparable to Pt/C both in acidic and alkaline media, high density of surface active sites, while its specific surface area is not so high	98
Fe-N-carbon	3.0 to 5.5	236	0.95 vs RHE	Kinetic current density is 7.40 mA cm^{-2} at 0.82 V, higher than that for Pt/C (6.30 mA cm^{-2} at 0.82 V), highly stability	99
Fe/carbon-N, Co/carbon-N	3.4 to 4.9	700 to 860	~0.8 V vs. RHE	Single cell PEMFC current density at 0.6 V vs. RHE: -0.1 A cm^{-2} for Fe/OMC-N; -0.06 A cm^{-2} for Co/OMC-N; -0.3 A cm^{-2} for commercial Pt/C.	102

3.3 Metal-free mesoporous electrocatalysts

The use of metal based catalysts brings about concerns about toxic metal pollution, irreplaceable or rare metal resources and hard-degraded substances. The crossover of anode fuels is one of challenges in fuel cells, and metal based catalysts are active toward both anode and cathode fuels. As a result,

fuel cell efficiency will be reduced owing to the undesirable oxidation reaction at cathode. Carbon materials are renewable and easy to handle, and are tolerant to anode fuels. They are promising materials for cathode catalysts to reach a high efficiency and reduce the cost. Furthermore, heteroatoms have different electronegativity and size from carbon atoms, and they can change the charge distribution and electronic properties of pure carbon materials[26, 75]. Tailoring carbon materials by introduction of heteroatoms to obtain metal-free catalysts with ideal ORR activity is a hot issue nowadays. In recent years, nitrogen-doped carbon with N-containing polymers, ammonia, as well as nitrogen gas as the nitrogen source or the source of both nitrogen and carbon has been developed, which possess good ORR activity [103-108]. Further developments on the combination of mesoporous carbon materials with heteroatoms doping make metal-free catalyst a potential substitution for Pt/C catalyst.

In a recent work, SBA-15 template is impregnated with pyrrole as both carbon and nitrogen sources via vaporization-capillary condensation in a vacuum container, and then forming the nitrogen-doped OMC after polymerization and etching [109]. The ORR current density at 0.9 V reaches 0.07, 0.09 and 0.12 mA cm^{-2} when the pyrolysis temperature was at 800 ºC, 900 ºC and 1000 ºC respectively. Furthermore it was found that nitrogen-activated carbon (C-N) is the active sites for the ORR because current density increases with C-N fraction. Zhang *et al.* developed a template-free simple method to fabricate nitrogen-doped porous carbon foam from melamine-formaldehyde foam by a two-step pyrolysis process: heating at 300 ºC in air and then at 1000 ºC in N_2 atmosphere [110]. This carbon foam (4.3 at.% N content) has small pore size below 5 nm and gives rise to a high specific surface area of 980 m^2 g^{-1}. Rotating disk electrode (RDE) voltammograms are used to investigate the ORR pathway of this carbon form. It reveals that the average electron transfer numbers is about 3.6 with little hydrogen peroxide generation. The ORR activity of carbon foam is slightly lower than that of Pt/C, but the methanol-tolerance is largely improved. Nanoporous carbon nanocables with carbon nanotubes as core and N-doped carbon as shell have been prepared by Jiang *et al*.[111] This core-shell catalyst has a specific surface area of 413 m^2 g^{-1} and pore diameter range from 1.7 to 4 nm. It demonstrates much higher ORR activity than the catalyst with core or shell only. It achieves four-electron transfer in ORR with high catalytic activity comparable with Pt/C and remarkable methanol tolerance. Nitrogen-doped hollow mesoporous carbon sphere (HMCS) was also prepared based on mesoporous silica spheres (MSS) as shown in Fig. 5 [112]. MSS is initially formed from tetraethylorthosilicate (TEOS) and trimethoxy(octadecyl) silane (C_{18}TMS), then HMCS is prepared after carbonization with the addition of nitrogen and carbon source and HF washing. The nitrogen sources for HMCS-1, HMCS-2 are glycine and lysine, respectively and glucose for HMCS-3 (no nitrogen doped). After forming hollow structure, specific surface area increases from 335 m^2 g^{-1} (MSS) to 451 m^2 g^{-1} (HMCS). Among the three prepared metal free catalysts toward ORR, HMCS-1 is the most active one, which displays comparable although inferior ORR activity to commercial Pt/C

catalyst (see Figs. 5E&5F). HMCS shows excellent methanol tolerant ability as it is inactive toward methanol, so it is a promising catalyst to replace Pt catalyst and achieve high efficiency. Moreover, another routine has been reported to prepare hollow nitrogen-doped carbon (HNC) as a simple, environmental friendly, economic and template-free synthesis method, as shown in Fig. 6 [113]. Aniline monomer was polymerized with the addition of $K_3[Fe(CN)_6]$ in ice bath (<5 ºC) for 24 h, followed by washing and carbonization to form the hollow and porous structure. Trace Fe (0.13 at.%) was left in HNC, with C, O, N content of 86.55, 11.87, 1.95 at.%. Fig. 6a and 6b demonstrate that HNC is close to commercial Pt/C in ORR activity. In addition, the HNC has advantages of better methanol crossover resistance and long-term durability in alkaline medium. This feature is excellent for methanol fuelled alkaline membrane fuel cells.

Dual elements doped mesoporous carbon was also prepared as ORR catalysts, such as B-, N-doped carbon nanofibers, S-, N-doped mesoporous carbon, O-, N-doped mesoporous carbon. Mesoporous carbon doped with N and O was fabricated by thermal treatment of PANI/SBA-15 and silica etching [64]. The heating temperature (600 ºC to 900 ºC) could affect the N and O contents in mesoporous carbon. Nitrogen atoms were observed to decrease with temperature rising. In contrast, O atoms would increase as the O is introduced from the mesoporous silica driven by the high temperature. Current density of ORR achieved from mesoporous N-, O-carbon synthesized at a pyrolysis temperature of 800 °C is larger than that of Pt/C. Qi Shi *et al.* prepare two kinds of B, N-codoped mesoporous carbon nanofibers, namely BNC_f-N and BNC_f-NA[114]. BNC_f-N is pyrolysed with the mixture of boric acid/urea under N_2, and BNC_f-NA is further treated under NH_3. The B-N-C sites can enhance ORR activity and demonstrate the synergistic effect of B, N-codoping. Raman and XPS spectra show the content of defect sites is enhanced after NH_3 activation. The relative amount of pyridinic-N, which is favourable for ORR, increased from 13 (BNC_f-N) to 41 at % (BNC_f-NA) after NH_3 activation, as shown in Fig. 7. The specific surface area increased from 24.7 (BNC_f-N) to 306.3 $m^2\ g^{-1}$ (BNC_f-NA) after NH_3 activation. Compared with commercial Pt/C catalysts, the metal free catalyst of BNC_f-NA shows high electrocatalytic efficiency, much better stability and methanol tolerance thus a promising alternative to Pt/C ORR catalyst.

To date, S-, N-doped porous carbon materials have been reported with different N and S sources, as shown in Table 3. Normally N and S co-doped carbon catalysts present larger number of electrons transfer compared to sole N or S doped carbon catalysts, leading to a high efficiency of ORR [115-117]. Sulphur atoms bonding with carbon are thiophene like structure, which are proved to improve the catalysts with sole nitrogen doping due to the synergistic effects originating from S and N atoms [116-118]. For example, S-, N-doped porous carbon foam exhibits ORR onset potential close to that of Pt/C, and its current density is higher with a limited-kinetics current density of 11.69 mA cm^{-2} at -0.40 V[119].

Rotating-disk voltammetry measurements show the number of electron transfer is 3.96, indicating a high-efficiency four-electron process with negligible formation of H_2O_2.

Table 3 Recently reported N-,S-co-doped mesoporous carbon catalysts for ORR.

Catalyst	Precursor (C, N, S)	Synthesis method and pyrolysis temperature	Specific surface area (m^2 g^{-1})	Content of S, N atoms	Ref.
N,S-mesoporous carbon	thiophene and pyrimidine	Mesoporous silica template and chemical vapour deposition, 700 ºC	1100	N: 4.7 at.% and S: 0.68 at.%	115
N,S-mesoporous carbon forms	Aniline, $Na_2S_2O_3$ and $(NH_4)_2S_2O_8$	Polymerization of aniline (shell) on the surface of sulphur sphere (core) and pyrolysis, 1000 ºC	133.56	N: 0.58 at.% and S: 1.0 at.%	116
N,S-mesoporous Graphene	Melamine and benzyl disulfide	Modified Hammer's method, colloidal silica template and pyrolysis, 900 ºC	157-220	N: 4.5 at.% and S: 2.0 at.%	117
N,S-mesoporous carbon/graphene nanosheets	cysteine	Mesoporous silica/graphene template and pyrolysis, 900 ºC	281	N: 2.97 wt.%; S: 0.89 wt.%	118
N,S-porous carbon forms	thiourea	Mesoporous silica template and pyrolysis, 1000 ºC	394	N: 6.53 wt.%; S: 2.88 wt.%	119
N,S-mesoporous carbon	phenothiazine (or indigo carmine)	Mesoporous silica template and pyrolysis, 750 ºC	855 (409)	N: 4.51 (6.38) wt.%; S: 4.12 (6.38) wt.%	120
N,S-porous carbon	1-allyl-2-thiourea	Silica nanospheres template and pyrolysis, 400~1000 ºC (900 ºC is optimal)	56.9 to 860.4	N/C (%): 2.5~26; S/C (%): 0.7~3.1	121

Gao *et al.* reported N-, S-, and P-tridoped porous carbon fabricated from pyrolysis of worst weed (*Eclipta prostrata*)[122]. Heteroatoms were directly introduced from the nature compounds of worst weed. The as-prepared tri-doped carbon consists of mesopores with diameter form 5 to 30 nm and a small number of macropores with diameter from 100-150 nm. Pore volumes and specific surface area reach 0.2676 cm^3 g^{-1} and 378.5 m^2 g^{-1}, respectively. This (N, S, P)-doped carbon achieves higher catalytic activity and better durability toward four-electron ORR in comparison with Pt/C catalyst.

Pyrolysis temperature is a vital factor in synthesis of heteroatoms doped mesoporous carbon, which can largely affect catalytic activity as well as transferred electrons number for ORR. The optimal pyrolysis temperature is around 900 ºC according to the reported works, and it may vary because of the different carbon and heteroatoms precursors used[64, 109, 111, 115-117, 119, 121]. If the pyrolysis temperature is too low, carbon sheath will not be adequately graphitized, thus the as-prepared mesoporous carbon is of poor electrical conductivity. If the pyrolysis temperature is too high, active sites in the as-

prepared mesoporous carbon will decrease due to the low heteroatoms doping level (density). Besides, specific surface area and pore volume of mesoporous carbon are also influenced by pyrolysis temperature. For these reasons, optimal preparation conditions are required to be investigated in order to make heteroatoms doped mesoporous carbon a potential substitute for commercial Pt/C catalyst with enhanced ORR activity, complete reduction product, long stability and methanol tolerance.

4. Fuel cell performance using electrocatalysts with mesoporous structure

Although many works reported superior performance of mesoporous catalysts toward anode and cathode reactions characterized by electrochemical measurements in three-electrode system, it was still required to be further verified by practical fuel cell performance. The three-electrode measurements are performed in bulk electrolyte with catalysts direct contacting to fuels. In fuel cell electrodes, liquid or gas fuels need to pass through the diffusion layer to reach the catalyst layer. As fuel cell is a more complicated system, many factors such as MEA fabrication (Nafion loading, gas diffusion layer, press process, etc.) and operation conditions (temperature, flow rate, humidity, etc.) will affect its current density except catalysts property, which probably diminish the superiority of mesoporous catalyst. For example, when Pt/mesoporous carbon (Pt/MC) is assembled at cathode in a H_2/O_2 fuel cell, the power density is higher than that of Pt/C cathode at 60 ºC [123]. However, the power densities become similar when operation temperature is 30 ºC. Ahn et al. found Pt particles in Pt/MC could deposit on two or more ordered carbon nanorods to share Nafion ionomer and electrolyte, thus less ionomer loading was required. The optimal Nafion loading at cathode for Pt/MC (10. wt%) is found to be lower than that for Pt/C (20 and 30 wt.%)[58]. In direct methanol fuel cell (DMFC) at 80 ºC, Pt/MC assembled in anode showed a maximum power density 8% higher than Pt/C, but Pt/MC assembled in cathode even showed slight lower maximum power density than Pt/C, and its best Nafion loading is 35% [77]. Flow rate of fuel also has different effects on Pt/MC and Pt/C. Recently Bruno *et al.* prepared Pt/MC with 5.3 nm in Pt particle size, which is 25% smaller than Pt/C (Vulcan carbon) [124]. When Pt/MC and Pt/C are used as cathode catalysts, the maximum power density of DMFC while using air reaches 30 mW cm^{-2} and 16 mW cm^{-2} respectively. They found that although mesoporous catalysts could reduce the mass transport losses promoting the water transportation, they would also promote the drying out of the MEA at high flow rates. As shown in Fig. 8A, the highest power is achieved at 100 sccm air flow, and the power will reduce as air flow increase to 150 sccm when using Pt/MC as cathode catalyst. On the contrary, in Fig. 8B, the power is observed to keep increasing with air flow up to 150 sccm when using Pt/C. Thus it is of vital importance for practical application of mesoporous catalysts to optimize MEA preparation and operation conditions of polymer electrolyte membrane fuel cells.

In most reported works, better results have been observed with mesoporous catalysts in fuel cell tests due to their merits as shown in Table 4. The Pt or Pt-alloy particles (~3 nm) can only be dispersed on the surface of microporous supports (< 2 nm in pore size), which aggregate easily and give rise to low ECSA. In addition, Nafion ionomer fails to enter pores with diameter smaller than 20 nm, showing poor contact between the metal nanoparticles and Nafion ionomer[125, 126]. On the contrary, the adequate pore size of mesoporous supports leads to more Pt dispersion and fuels accessible in mesopores[126]. Pt particles in mesopores could share Nafion ionomer and fuels, thus less ionomer loading was required[58]. The H_2O produced by electrochemical reactions can easily transfer from the catalyst layer to the gas diffusion layer with less space occupied by ionomer. Thus mesoporous structure is favourable for mass transport in catalyst layer[126, 127]. On the anode side, when assembled with PtRu/C, maximum power density of DMFC reaches 17 W g_{Pt}^{-1} (34 mW cm^{-2}) and 26 W g_{Pt}^{-1} (61 mW cm^{-2}) at 30 ºC and 60 ºC respectively [59]. It increases to 31 W g_{Pt}^{-1} (40 mW cm^{-2}) at 30 ºC and 45 W g_{Pt}^{-1} (67 mW cm^{-2}) at 60 ºC when assembled with PtRu/MC, attributing to the fast oxidation rate and enhanced mass transport of methanol with mesoporous catalysts. Song *et al.* report that ultrafine porous carbon fiber with pores (5-30 nm diameters) can be straightforward formed after carbon fiber is oxidized at 280 ºC and subsequently carbonized at 1400 ºC [128]. Carbon fiber is prepared via electro-spinning of polyacrylonitrile/polymethyl methacrylate (PAN/PMMA) blend solution on aluminium foil. Platinum supported on this carbon fiber makes the power density 1.25 times higher than commercial Pt/C in single fuel cell tests at room temperature. On the cathode side, mesoporous carbon doped with heteroatoms or Fe, Co have shown better performance in fuel cells than Pt/C[86, 100, 109]. Mesoporous carbon doped with Fe and N achieves power density of 227 mW cm^{-2} in an anion-exchange-membrane based alkaline methanol fuel cell, which is higher than that of 195 mW cm^{-2} achieved from Pt/C[100]. Wan *et al.* reported that their N-doped mesoporous carbon exhibited twice higher power density of DMFC than Pt/C[109] The reason was not only that N-doped mesoporous carbon showed higher ORR activity, but also that it was inactive toward methanol thus eliminating the negative effect of the methanol crossover .

Table 4 Comparisons between mesoporous catalysts and traditional carbon supported Pt (Pt alloys) applied in fuel cell electrodes.

	Mesoporous catalysts	Traditional carbon supported Pt (Pt alloys)
Pt dispersion	Uniform with high specific area	Easy to aggregate
Mass transport of fuels	Good access to fuels due to adequate pore sizes and volumes	Pore size too small to obtain adequate fuels, pore space tends to be filled with H_2O to slow down mass transport
MEA preparation	Applicable to alkaline and acidic membranes, less ionomer loading required	Applicable to alkaline and acidic membranes, normally 20~40 wt.% of ionomer loading
Durability	Enhanced thermal, chemical and	Degeneration of carbon black, not tolerant

	mechanical stability, tolerant to methanol crossover (heteroatoms doped carbon)	to methanol crossover
Price	Cost-effective, noble-metal-free	High price due to the use of noble metal

5. Summary and outlook

This mini-review summarises recent development and exciting researches in the application of mesoporous materials as anode and cathode electro-catalysts in polymer membrane fuel cells. For anode catalysts, mesoporous Pt based metals have been prepared via template-assisted reduction or sputtering deposition methods. They have shown increased specific surface area, improved electrochemical activity and poisoning tolerance due to the optimal mesoporous structure. More works have been done to obtain high-performance catalysts with metals supported on mesoporous materials. The developments of mesoporous carbon and other inorganic compounds have solved the problem of poor electrical conductivity in silica-based mesoporous materials and broaden their applications in electrocatalysts. For cathode catalysts, Pt-based mesoporous catalysts have achieved enhanced specific mass activity and stability in comparison with commercial Pt/C, but they are not tolerant to methanol crossover. On the contrary, heteroatoms doped mesoporous carbon are inactive toward anode fuel (methanol), so they are presented to have improved durability and high fuel cell efficiency, though their ORR activities are slightly lower than those of Pt-based mesoporous catalysts. Additionally, various kinds of organic compounds and even nature biomass can be used as sources to prepare heteroatoms doped mesoporous carbon, leading to a great reduction of catalysts cost. The mesoporous supporting materials have some advantages over commercial carbon supports, including (1) several times larger specific surface area and high accessible surface area to support metal deposition, (2) good catalyst–support interaction, (3) high electrical conductivity, (4) good mass transfer of fuels in pores, (5) uniform and small metallic nanoparticles dispersion and (6) strong corrosion resistance. As a result, mesoporous electrocatalysts have shown better performance than commercial Pt/C. However, mesoporous anode catalysts without noble metals and mesoporous catalysts for nitrogen-containing fuels oxidation have not been intensively studied. It was found that Pt-based catalysts are easily poisoned by the adsorbed N_{ads}, and thus limits the current density and service life [129-131]. As mesoporous catalysts have demonstrated both activity and CO-tolerance improvement, they may also be developed as a strategy of noble metal free and N_{ads}-tolerance catalysts as anode materials for fuel cells in the future.

Acknowledgements

The authors thank EPSRC Supergen fuel cell project (EP/G030995/1) for funding. One of the authors (Xu) gratefully acknowledges the China Scholarship Council (CSC) for financial support.

References

1. N. V. Rees and R. G. Compton, *Energy Environ. Sci.*, 2011, **4**, 1255-1260.
2. L. An, T. S. Zhao and Y. S. Li, *Renew. Sust. Energ. Rev.*, 2015, **50**, 1462-1468.
3. R. Lan, S. W. Tao and J. T. S. Irvine, *Energy Environ. Sci.*, 2010, **3**, 438-441.
4. E. Antolini, J. R. C. Salgado and E. R. Gonzalez, *Appl. Catal. B Environ.*, 2006, **63**, 137-149.
5. J. Jiang and A. Kucernak, *J. Electroanal. Chem.*, 2009, **630**, 10-18.
6. A. Serov and C. Kwak, *Appl. Catal. B Environ.*, 2010, **98**, 1-9.
7. X. Luo, J. Wang, M. Dooner and J. Clarke, *Appl. Energy*, 2015, **137**, 511-536.
8. R. Lan and S. W. Tao, *J. Power Sources*, 2011, **196**, 5021-5026.
9. H. Zhang, W. Xu, D. Feng, Z. Liu and Z. Wu, *Bioresour. Technol.*, 2016, **203**, 56-61.
10. T. Hua, R. Ahluwalia, L. Eudy, G. Singer, B. Jermer, N. Asselin-Miller, S. Wessel, T. Patterson and J. Marcinkoski, *J. Power Sources*, 2014, **269**, 975-993.
11. J. Wang, *Energy*, 2015, **80**, 509-521.
12. US Department of Energy, Technical System Targets: Onboard Hydrogen Storage for Light-Duty Fuel Cell Vehicles. http://energy.gov/sites/prod/files/2015/01/f19/fcto_myrdd_table_onboard_h2_storage_systems_doe_targets_ldv.pdf. (Accessed March 2016).
13. N. Guerrero Moreno, M. Cisneros Molina, D. Gervasio and J. F. Pérez Robles, *Renew. Sust. Energ. Rev.*, 2015, **52**, 897-906.
14. G. Øye, J. Sjöblomb and M. Stöckerc, *Adv. Colloid Interface Sci.*, 2001, **89-90**, 439-466.
15. Y.-P. Zhu and Z.-Y. Yuan, *Mesoporous Organic-Inorganic Non-Siliceous Hybrid Materials*, Springer-Verlag Berlin Heidelberg, 2015.
16. N. Linares, A. M. Silvestre-Albero, E. Serrano, J. Silvestre-Albero and J. Garcia-Martinez, *Chem. Soc. Rev.*, 2014, **43**, 7681-7717.
17. S. P. Jiang, *Solid State Ion.*, 2014, **262**, 307-312.
18. S. P. Jiang, *J. Mater. Chem. A*, 2014, **2**, 7637-7655.
19. J. Zeng, B. He, K. Lamb, R. De Marco, P. K. Shen and S. P. Jiang, *ACS Appl. Mater. Interfaces*, 2013, **5**, 11240-11248.
20. J. Park and D. Kim, *Int. J. Hydrog. Energy*, 2014, **39**, 1063-1070.
21. D. Schneider, D. Mehlhorn, P. Zeigermann, J. Karger and R. Valiullin, *Chem. Soc. Rev.*, 2016, **45**, 3439-3467.
22. J. Karger and R. Valiullin, *Chem. Soc. Rev.*, 2013, **42**, 4172-4197.
23. K. Vignarooban, J. Lin, A. Arvay, S. Kolli, I. Kruusenberg, K. Tammeveski, L. Munukutla and A. M. Kannan, *Chinese J. Catal.*, 2015, **36**, 458-472.
24. P. Zhang, H. Zhu and S. Dai, *ChemCatChem*, 2015, **7**, 2788-2805.
25. P. Trogadas, V. Ramani, P. Strasser, T. F. Fuller and M.-O. Coppens, *Angew. Chem. Int. Edit.*, 2016, **55**, 122-148.
26. L. Dai, Y. Xue, L. Qu, H.-J. Choi and J.-B. Baek, *Chem. Rev.*, 2015, **115**, 4823-4892.
27. K. N. Wood, R. O'Hayre and S. Pylypenko, *Energy Environ. Sci.*, 2014, **7**, 1212-1249.
28. W. Li, J. Liu and D. Zhao, *Nat. Rev. Mater.*, 2016, **1**, 16023.
29. C. Zhong, W. B. Hu and Y. F. Cheng, *J. Mater. Chem. A*, 2013, **1**, 3216-3238.
30. T. L. Lomocso and E. A. Baranova, *Electrochim. Acta*, 2011, **56**, 8551-8558.
31. H. Li, H. Lin, Y. Hu, H. Li, P. Li and X. Zhou, *J. Mater. Chem.*, 2011, **21**, 18447-18453.
32. Y. Ma, R. Wang, H. Wang, V. Linkov and S. Ji, *Phys. Chem. Chem.Phys.*, 2014, **16**, 3593-3602.
33. L.-X. Ding, G.-R. Li, Z.-L. Wang, Z.-Q. Liu, H. Liu and Y.-X. Tong, *Chem. Eur. J.*, 2012, **18**, 8386–8391.
34. E. A. Franceschini, G. A. Planes, F. J. Williams, G. J. A. A. Soler-Illia and H. R. Corti, *J. Power Sources*, 2011, **196**, 1723-1729.

35. H. Wang, H. Y. Jeong, M. Imura, L. Wang, L. Radhakrishnan, N. Fujita, T. Castle, O. Terasaki and Y. Yamauchi, *J. Am. Chem. Soc.*, 2011, **133**, 14526-14529.
36. L. Wang and Y. Yamauchi, *Chem. Eur. J.*, 2011, **17**, 8810-8815.
37. L.-X. Ding, G.-R. Li, Z.-L. Wang, Z.-Q. Liu, H. Liu and Y.-X. Tong, *Chem. Eur. J.*, 2012, **18**, 8386-8391.
38. A. Serrà, E. Gómez and E. Vallés, *Int. J. Hydrog. Energy*, 2015, **40**, 8062-8070.
39. A. Serrà, M. Montiel, E. Gómez and E. Vallés, *Nanomaterials*, 2014, **4**, 189.
40. J. Thepkaew, S. Therdthianwong, A. Therdthianwong, A. Kucernak and N. Wongyao, *Int. J. Hydrog. Energy*, 2013, **38**, 9454-9463.
41. A. Takai, T. Saida, W. Sugimoto, L. Wang, Y. Yamauchi and K. Kuroda, *Chem. Mater.*, 2009, **21**, 3414-3423.
42. E. A. Franceschini, M. M. Bruno, F. J. Williams, F. A. Viva and H. R. Corti, *ACS Appl. Mater. Interfaces*, 2013, **5**, 10437-10444.
43. E. Antolini, *Appl. Catal. B Environ.*, 2009, **88**, 1-24.
44. H. Huang and X. Wang, *J. Mater. Chem. A*, 2014, **2**, 6266-6291.
45. C. Galeano, J. C. Meier, M. Soorholtz, H. Bongard, C. Baldizzone, K. J. J. Mayrhofer and F. Schüth, *ACS Catal.*, 2014, **4**, 3856-3868.
46. X. Yuan, X.-L. Ding, C.-Y. Wang and Z.-F. Ma, *Energy Environ. Sci.*, 2013, **6**, 1105-1124.
47. D. Banham, F. Feng, T. Fürstenhaupt, K. Pei, S. Ye and V. Birss, *J. Power Sources*, 2011, **196**, 5438-5445.
48. G. Sasikumar, J. W. Ihm and H. Ryu, *Electrochim. Acta*, 2004, **50**, 601-605.
49. W. Zhang, J. Chen, G. F. Swiegers, Z.-F. Ma and G. G. Wallace, *Nanoscale*, 2010, **2**, 282-286.
50. F. Han, X. Wang, J. Lian and Y. Wang, *Carbon*, 2012, **50**, 5498-5504.
51. C. Zhang, L. Xu, N. Shan, T. Sun, J. Chen and Y. Yan, *ACS Catal.*, 2014, **4**, 1926-1930.
52. L. Zhao, Z.-B. Wang, X.-L. Sui and G.-P. Yin, *J. Power Sources*, 2014, **245**, 637-643.
53. X. Li, W. Liu, J. Ma, Y. Wen and Z. Wu, *Appl. Catal. B Environ.*, 2015, **179**, 239-248.
54. E. Li and V. Rudolph, *Energy Fuels*, 2008, **22**, 145-149.
55. R. Ryoo, S. H. Joo and S. Jun, *J. Phys. Chem. B*, 1999, **103**, 7743-7746.
56. K. L. Yeung and W. Han, *Catal. Today*, 2014, **236, Part B**, 182-205.
57. X. He, Y. Zhang, C. Zhu, H. Huang, H. Hu, Y. Liu and Z. Kang, *New J. Chem.*, 2015, **39**, 8667-8672.
58. C.-Y. Ahn, J.-Y. Cheon, S.-H. Joo and J. Kim, *J. Power Sources*, 2013, **222**, 477-482.
59. M. M. Bruno, M. A. Petruccelli, F. A. Viva and H. R. Corti, *Int. J. Hydrog. Energy*, 2013, **38**, 4116-4123.
60. S.-Y. Lee, B.-J. Kim and S.-J. Park, *Energy*, 2014, **66**, 70-76.
61. S. Pérez-Rodríguez, N. Rillo, M. J. Lázaro and E. Pastor, *Appl. Catal. B Environ.*, 2015, **163**, 83-95.
62. C. a. Cao, X. Zhuang, Y. Su, Y. Zhang, F. Zhang, D. Wu and X. Feng, *Polym. Chem.*, 2014, **5**, 2057-2064.
63. M. Sevilla, L. Yu, T. P. Fellinger, A. B. Fuertes and M.-M. Titirici, *RSC Adv.*, 2013, **3**, 9904-9910.
64. R. Silva, D. Voiry, M. Chhowalla and T. Asefa, *J. Am. Chem. Soc.*, 2013, **135**, 7823-7826.
65. G. Wu, K. L. More, C. M. Johnston and P. Zelenay, *Science*, 2011, **332**, 443-447.
66. L.-M. Zhang, Z.-B. Wang, J.-J. Zhang, X.-L. Sui, L. Zhao and D.-M. Gu, *Carbon*, 2015, **93**, 1050-1058.
67. P. Song, L. Zhu, X. Bo, A. Wang, G. Wang and L. Guo, *Electrochim. Acta*, 2014, **127**, 307-314.
68. K. Wang, Y. Wang, Z. Liang, Y. Liang, D. Wu, S. Song and P. Tsiakaras, *Appl. Catal. B Environ.*, 2014, **147**, 518-525.
69. M. Lei, T. Z. Yang, W. J. Wang, K. Huang, R. Zhang, X. L. Fu, H. J. Yang, Y. G. Wang and W. H. Tang, *Int. J. Hydrog. Energy*, 2013, **38**, 205-211.
70. X. Zhang, J. He, T. Wang, M. Liu, H. Xue and H. Guo, *J. Mater. Chem. A*, 2014, **2**, 3072-3082.

71. M. A. Hoque, D. C. Higgins, F. M. Hassan, J.-Y. Choi, M. D. Pritzker and Z. Chen, *Electrochim. Acta*, 2014, **121**, 421-427.
72. M. P. Gurrola, M. Guerra-Balcázar, L. Álvarez-Contreras, R. Nava, J. Ledesma-García and L. G. Arriaga, *J. Power Sources*, 2013, **243**, 826-830.
73. M. Yang, Z. Cui and F. J. DiSalvo, *Phys. Chem. Chem. Phys.*, 2013, **15**, 1088-1092.
74. M. Yang, R. Guarecuco and F. J. DiSalvo, *Chem. Mater.*, 2013, **25**, 1783-1787.
75. J. Zhang, Z. Xia and L. Dai, *Sci. Adv.*, 2015, **1**, e1500564.
76. P. Liu, J. Kong, Y. Liu, Q. Liu and H. Zhu, *J. Power Sources*, 2015, **278**, 522-526.
77. F. A. Viva, M. M. Bruno, E. A. Franceschini, Y. R. J. Thomas, G. Ramos Sanchez, O. Solorza-Feria and H. R. Corti, *Int. J. Hydrog. Energy*, 2014, **39**, 8821-8826.
78. D. J. You, X. Jin, J. H. Kim, S.-A. Jin, S. Lee, K. H. Choi, W. J. Baek, C. Pak and J. M. Kim, *Int. J. Hydrog. Energy*, 2015, **40**, 12352-12361.
79. J.-M. Oh, J. Park, A. Kumbhar, D. Smith Jr and S. Creager, *Electrochim. Acta*, 2014, **138**, 278-287.
80. M. Yang, Z. Cui and F. J. DiSalvo, *Phys. Chem. Chem.Phys.*, 2013, **15**, 7041-7044.
81. Z. Cui, R. G. Burns and F. J. DiSalvo, *Chem. Mater.*, 2013, **25**, 3782-3784.
82. A. H. A. Monteverde Videla, L. Zhang, J. Kim, J. Zeng, C. Francia, J. Zhang and S. Specchia, *J. Appl. Electrochem.*, 2012, **43**, 159-169.
83. L. Zhang, J. Kim, E. Dy, S. Ban, K.-c. Tsay, H. Kawai, Z. Shi and J. Zhang, *Electrochim. Acta*, 2013, **108**, 814-819.
84. L. Zhang, J. Kim, E. Dy, S. Ban, K.-c. Tsay, H. Kawai, Z. Shi and J. Zhang, *Electrochim. Acta*, 2013, **108**, 480-485.
85. H.-W. Liang, W. Wei, Z.-S. Wu, X. Feng and K. Müllen, *J. Am. Chem. Soc.*, 2013, **135**, 16002-16005.
86. M. E. Hamzehie, L. Samiee, M. Fattahi, A. A. Seifkordi, F. Shoghi and A. Maghsodi, *Renew. Energy*, 2015, **77**, 558-570.
87. Y.-L. Liu, X.-Y. Xu, P.-C. Sun and T.-H. Chen, *Int. J. Hydrog. Energy*, 2015, **40**, 4531-4539.
88. A. L. Ong, S. Saad, R. Lan, R. J. Goodfellow and S. W. Tao, *J. Power Sources*, 2011, **196**, 8272-8279.
89. H. A. Gasteiger, A. Weber, K. Shinohara, H. Uchida, S. Mitsushima, T. J. Schmidt, S. R. Narayanan, V. Ramani, T. Fuller, M. Edmundson, P. Strasser, R. Mantz, J. Fenton, F. N. Buchi, D. C. Hansen, D. L. Jones, C. Coutanceau, K. SwiderLyons and K. A. Perry, *Polymer Electrolyte Fuel Cells 13 (PEFC 13)*, The Electrochemical Society, Pennington, 2013.
90. J. R. Varcoe, P. Atanassov, D. R. Dekel, A. M. Herring, M. A. Hickner, P. A. Kohl, A. R. Kucernak, W. E. Mustain, K. Nijmeijer, K. Scott, T. Xu and L. Zhuang, *Energy Environ. Sci.*, 2014, **7**, 3135-3191.
91. R. Lan and S. W. Tao, *Electrochem. Solid State Lett.*, 2010, **13**, B83-B86.
92. S. Lu, J. Pan, A. Huang, L. Zhuang and J. Lu, *Proc. Natl. Acad. Sci. USA*, 2008, **105**, 20611–20614.
93. J. Xiao, X. Bian, L. Liao, S. Zhang, C. Ji and B. Liu, *ACS Appl. Mater. Interfaces*, 2014, **6**, 17654-17660.
94. H. Huang, Q. Wang, Q. Wei and Y. Huang, *Int. J. Hydrog. Energy*, 2015, **40**, 6072-6084.
95. B. Chen, R. Li, G. Ma, X. Gou, Y. Zhu and Y. Xia, *Nanoscale*, 2015, **7**, 20674-20684.
96. P. Ganesan, M. Prabu, J. Sanetuntikul and S. Shanmugam, *ACS Catal.*, 2015, **5**, 3625-3637.
97. X. Tong, X. Xia, C. Guo, Y. Zhang, J. Tu, H. J. Fan and X.-Y. Guo, *J. Mater. Chem. A*, 2015, **3**, 18372-18379.
98. L. Lin, Q. Zhu and A.-W. Xu, *J. Am. Chem. Soc.*, 2014, **136**, 11027-11033.
99. X.-H. Yan and B.-Q. Xu, *J. Mater. Chem. A*, 2014, **2**, 8617-8622.
100. J. Chen, X. Cui and W. Zheng, *Catal. Commun.*, 2015, **60**, 37-41.
101. D.-S. Yang, M. Y. Song, K. P. Singh and J.-S. Yu, *Chem. Commun.*, 2015, **51**, 2450-2453.

102. J. K. Dombrovskis, H. Y. Jeong, K. Fossum, O. Terasaki and A. E. C. Palmqvist, *Chem. Mater.*, 2013, **25**, 856-861.
103. R. L. Arechederra, K. Artyushkova, P. Atanassov and S. D. Minteer, *ACS Appl. Mater. Interfaces*, 2010, **2**, 3295-3302.
104. Z. Chen, D. Higgins and Z. Chen, *Carbon*, 2010, **48**, 3057-3065.
105. Y. Zheng, Y. Jiao, J. Chen, J. Liu, J. Liang, A. Du, W. Zhang, Z. Zhu, S. C. Smith, M. Jaroniec, G. Q. Lu and S. Z. Qiao, *J. Am. Chem. Soc.*, 2011, **133**, 20116-20119.
106. L. Qu, Y. Liu, J.-B. Baek and L. Dai, *ACS Nano*, 2010, **4**, 1321-1326.
107. J. P. McClure, J. D. Thornton, R. Jiang, D. Chu, J. J. Cuomo and P. S. Fedkiw, *J. Electrochem. Soc.*, 2012, **159**, F733-F742.
108. S. Shrestha and W. E. Mustain, *J. Electrochem. Soc.*, 2010, **157**, B1665-B1672.
109. K. Wan, G.-F. Long, M.-Y. Liu, L. Du, Z.-X. Liang and P. Tsiakaras, *Appl. Catal. B Environ.*, 2015, **165**, 566-571.
110. H. Zhang, Y. Zhou, C. Li, S. Chen, L. Liu, S. Liu, H. Yao and H. Hou, *Carbon*, 2015, **95**, 388-395.
111. W.-J. Jiang, J.-S. Hu, X. Zhang, Y. Jiang, B.-B. Yu, Z.-D. Wei and L.-J. Wan, *J. Mater. Chem. A*, 2014, **2**, 10154-10160.
112. J. Yan, H. Meng, F. Xie, X. Yuan, W. Yu, W. Lin, W. Ouyang and D. Yuan, *J. Power Sources*, 2014, **245**, 772-778.
113. R. Wu, S. Chen, Y. Zhang, Y. Wang, W. Ding, L. Li, X. Qi, X. Shen and Z. Wei, *J. Power Sources*, 2015, **274**, 645-650.
114. Q. Shi, Y. Lei, Y. Wang, H. Wang, L. Jiang, H. Yuan, D. Fang, B. Wang, N. Wu and Y. Gou, *Curr. Appl. Phys.*, 2015, **15**, 1606-1614.
115. J. Xu, Y. Zhao, C. Shen and L. Guan, *ACS Appl. Mater. Interfaces*, 2013, **5**, 12594-12601.
116. S. Jiang, Y. Sun, H. Dai, J. Hu, P. Ni, Y. Wang and Z. Li, *Electrochim. Acta*, 2015, **174**, 826-836.
117. J. Liang, Y. Jiao, M. Jaroniec and S. Z. Qiao, *Angew. Chem. Int. Edit.*, 2012, **51**, 11496-11500.
118. P. Xu, D. Wu, L. Wan, P. Hu and R. Liu, *J. Colloid Interface Sci.*, 2014, **421**, 160-164.
119. Z. Liu, H. Nie, Z. Yang, J. Zhang, Z. Jin, Y. Lu, Z. Xiao and S. Huang, *Nanoscale*, 2013, **5**, 3283-3288.
120. V. Perazzolo, C. Durante, R. Pilot, A. Paduano, J. Zheng, G. A. Rizzi, A. Martucci, G. Granozzi and A. Gennaro, *Carbon*, 2015, **95**, 949-963.
121. Y. Li, H. Zhang, Y. Wang, P. Liu, H. Yang, X. Yao, D. Wang, Z. Tang and H. Zhao, *Energy Environ. Sci.*, 2014, **7**, 3720-3726.
122. S. Gao, X. Wei, H. Liu, K. Geng, H. Wang, H. Moehwald and D. Shchukin, *J. Mater. Chem. A*, 2015, **3**, 23376-23384.
123. C. Alegre, M. E. Gálvez, R. Moliner, V. Baglio, A. S. Aricò and M. J. Lázaro, *Appl. Catal. B Environ.*, 2014, **147**, 947-957.
124. M. M. Bruno, F. A. Viva, M. A. Petruccelli and H. R. Corti, *J. Power Sources*, 2015, **278**, 458-463.
125. V. Rao, P. A. Simonov, E. R. Savinova, G. V. Plaksin, S. V. Cherepanova, G. N. Kryukova and U. Stimming, *J. Power Sources*, 2005, **145**, 178-187.
126. J. B. Xu and T. S. Zhao, *RSC Adv.*, 2013, **3**, 16-24.
127. H. Chang, S. H. Joo and C. Pak, *J. Mater. Chem.*, 2007, **17**, 3078-3088.
128. J. Song, G. Li and J. Qiao, *Electrochim. Acta*, 2015, **177**, 174-180.
129. J. A. Herron, P. Ferrin and M. Mavrikakis, *J. Phys. Chem. C*, 2015, **119**, 14692-14701.
130. L. A. Diaz and G. G. Botte, *Electrochim. Acta*, 2015, **179**, 529-537.
131. L. A. Diaz and G. G. Botte, *Electrochim. Acta*, 2015, **179**, 519-528.

Figures and captions

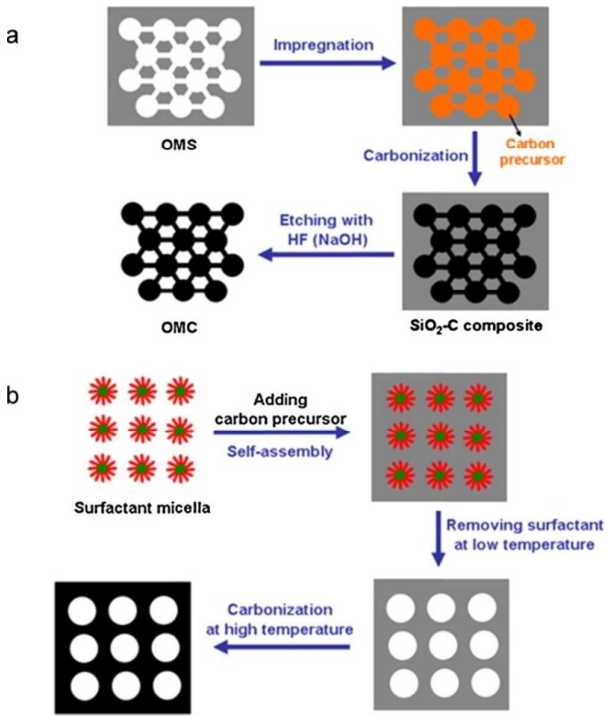

Fig. 1 Schematic diagrams of (a) hard template and (b) soft template methods to prepare mesoporous carbon. Reproduced with permission from ref. 56. Copyright 2014, Elsevier.

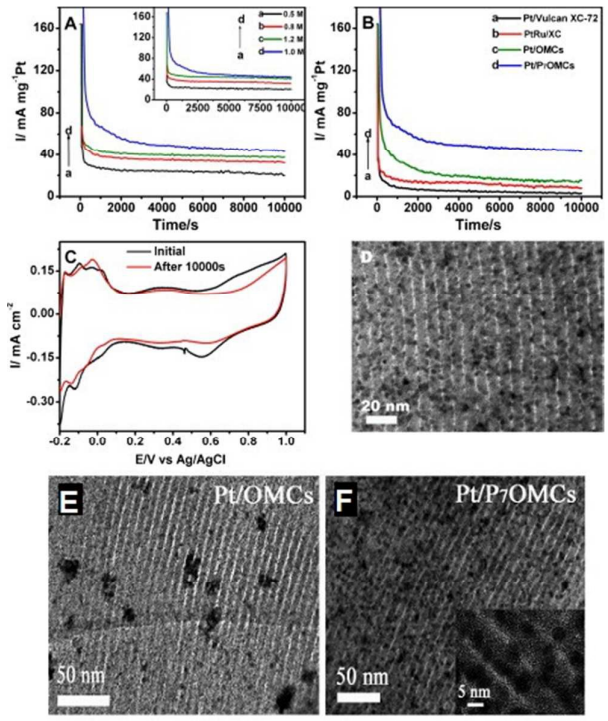

Fig. 2 (A) Chronoamperometry curves of Pt/P_7OMCs at different oxidation voltages: a) 0.5, b) 0.6, c) 0.8, d) 0.7 V (inset: with different concentrations of methanol at 0.7 V) in solution of 0.5 M H_2SO_4 + 1.0 M CH_3OH. (B) Chronoamperometry curves of Pt/Vulcan XC-72, PtRu/XC, Pt/OMCs and Pt/P_7OMCs recorded at 0.7 V. Scan rate: 50 mV s^{-1}. (C) CVs of Pt/P_7OMCs in 0.5 M H_2SO_4 before and after 10000 s stability test. TEM image of (D) Pt/P_7OMCs after 10000 s stability test; (E) Pt/OMCs and (F) Pt/P_7OMCs. Reproduced with permission from ref. 67. Copyright 2014, Elsevier.

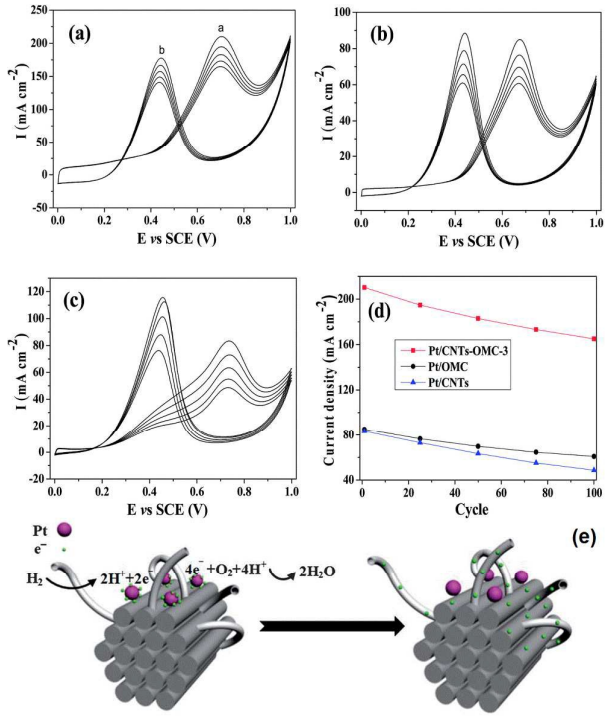

Fig. 3 Long-term stability of (a) Pt/CNTs–OMC, (b) Pt/OMC and (c) Pt/CNTs in 1.0 mol L^{-1} H_2SO_4 + 2.0 mol L^{-1} CH_3OH with a scan rate of 50 mV s^{-1} for 100 cycles and (d) the current density tendency of Pt/CNTs–OMC, Pt/OMC and Pt/CNTs in the forward scan with the increasing cycle number. (e) Schematic of electron transport in Pt/CNTs–OMC. Reproduced from Ref. 70 with permission from the Royal Society of Chemistry.

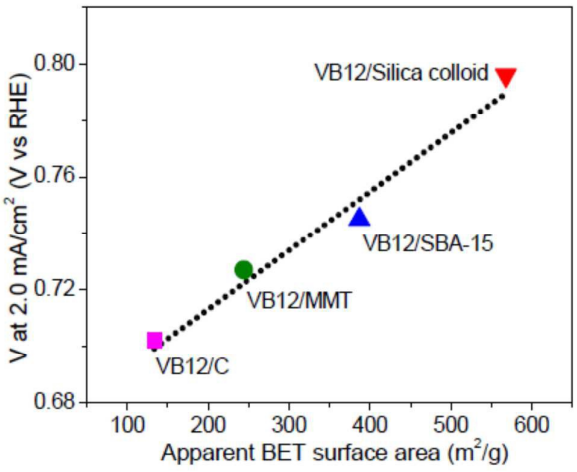

Fig. 4 The correlation between catalyst activity and apparent BET surface areas of the C-N-Co catalysts. Reproduced with permission from ref. 85. Copyright 2013, American Chemical Society.

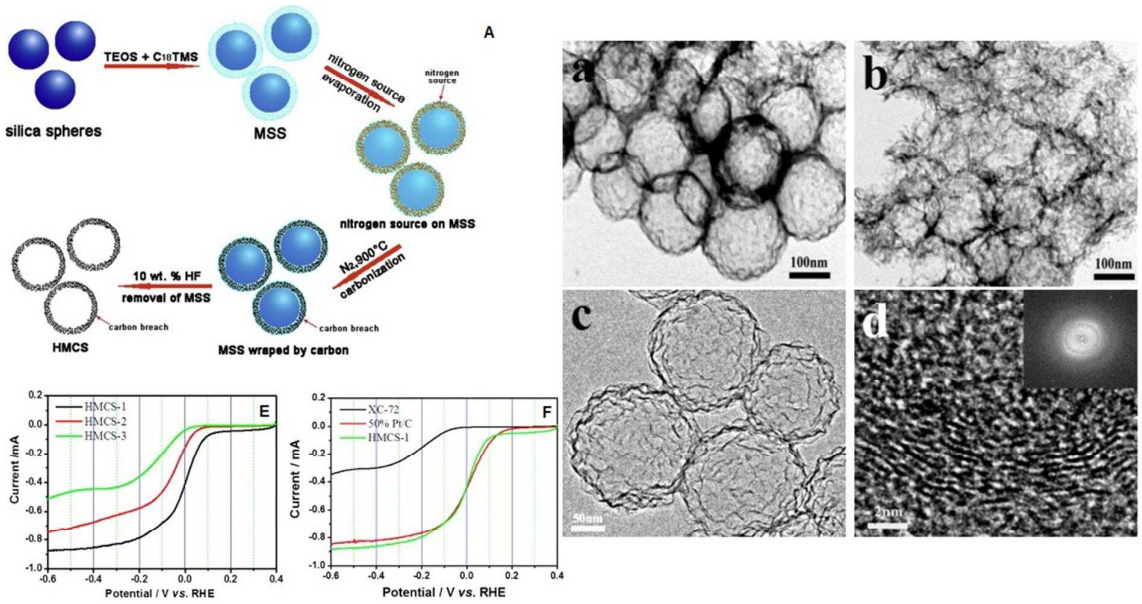

Fig. 5 (A) Schematic illustration of the formation of HMCS; TEM micrographs of HMCS-1 (a) and HMCS-2 (b); HRTEM micrographs (c and d) and SAED (inset in d) of HMCS-1; ORR polarization curves of HMCS (E) and Pt/C (F) in O_2 saturated 0.1 M KOH solution, sweep rate: 10 mV s^{-1}, rotation speed: 1600 rpm. Reproduced with permission from ref. 112. Copyright 2014, Elsevier.

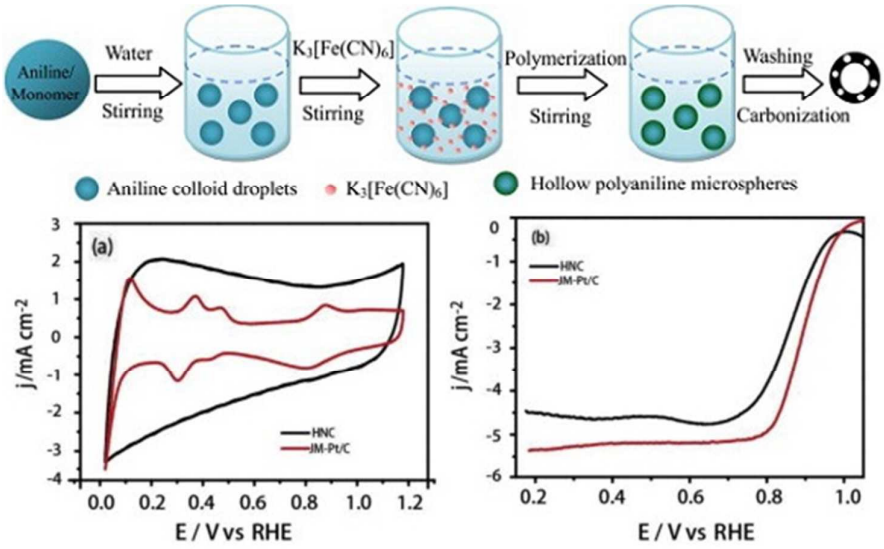

Fig. 6 Schematic representation of the synthesis of hollow nitrogen-doped carbon; (a) CV curves of HNC and commercial Pt/C catalysts in 0.1 M KOH at a sweep rate of 50 mV s^{-1}. (b) LSV curves of HNC and commercial Pt/C catalysts in O_2 saturated 0.1 M KOH at a sweep rate of 10 mV s^{-1} and 1600 rpm rotating speed. Reproduced with permission from ref. 113. Copyright 2015, Elsevier.

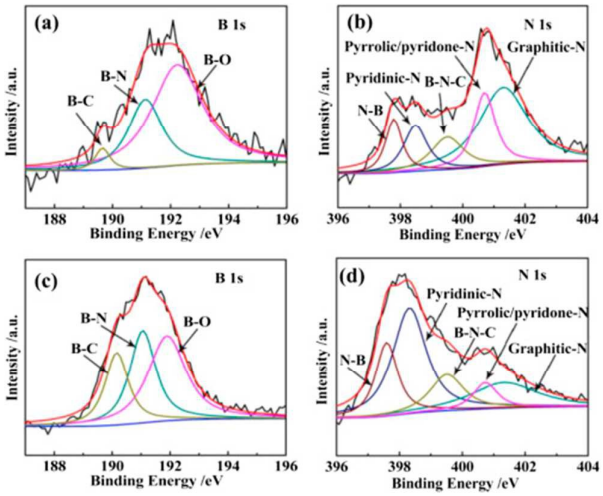

Fig. 7 B 1s and N 1s XPS spectra of (a and b) BNC_f-N and (c and d) BNC_f-NA. Reproduced with permission from ref. 114. Copyright 2015, Elsevier.

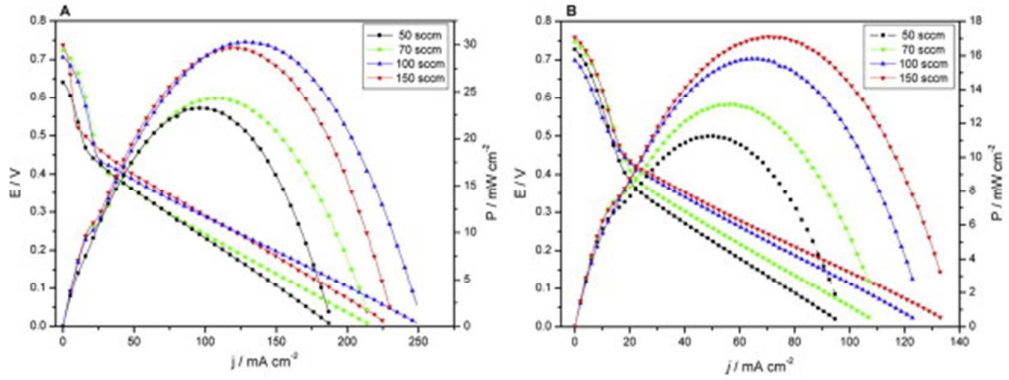

Fig. 8 Polarization and power curves at different Air flows for (A) Pt/mesoporous carbon and (B) Pt/Vulcan carbon at 60 ºC and 1 M methanol as anode fuel. Reproduced with permission from ref. 124. Copyright 2015, Elsevier.

Manuscript ID: TA-REV-06-2016-005304

Title: **Recent progress on electrocatalysts with mesoporous structure for application in polymer electrolyte membrane fuel cells**

Corresponding Author: Prof. Shanwen Tao

All Authors: Wei Xu, Zucheng Wu and Shanwen Tao

Journal: Journal of Materials Chemistry A

TOC:

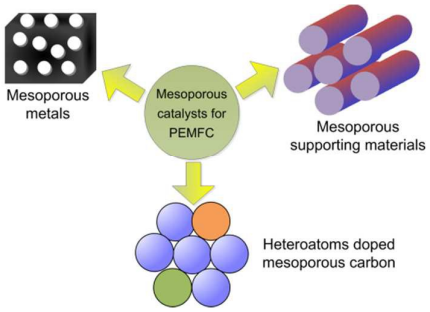

This paper summarizes the recent progress of mesoporous materials as electrocatalysts for applications in polymer electrolyte membrane fuel cells.